This article has been accepted for publication in a future issue of this journal, but has not been fully edited. Content may change prior to final publication. Citation information: DOI 10.1109/TAP.2022.3161358, IEEE Transactions on Antennas and Propagation

Communication

Reconfigurable UWB Circularly Polarized Slot Antenna with Three Modes of Operation and Continuous Tuning Range

Sirous Bahrami, Gholamhosein Moloudian, Ho-Jin Song, *Senior Member, IEEE*, and John L. Buckley, *Member, IEEE* .

***Abstract*—In this paper, a tunable circularly polarized antenna with a reconfigurable integrated feed network is proposed for cognitive radio applications. The integrated feed network is composed of an ultra-wideband (UWB) band-pass filter (BPF), a continuously tunable T-shaped resonator, and an L-shaped microstrip line. The feed network employs 3 PIN diodes to switch between different RF paths, resulting in 3 modes of operation: an ultra-wideband mode (3.5-8.5 GHz), a narrowband bandpass (BP) mode and a narrowband bandstop (BS) mode. The continuous tuning range of the bandpass/bandstop narrowband mode is realized by two DC-controlled varactor diodes. The stand-alone antenna attains a -10 dB impedance bandwidth of 92.3 % (3.5-9.5 GHz), while it attains an Axial Ratio (AR) bandwidth of 88.3 % (3.1-8 GHz) in its wideband mode. The overlapped bandwidth (matching and AR) of the reconfigurable antenna is 78.2 % (3.5-8 GHz). The communicating state covers 80% of the sensing spectrum while maintaining circularly polarized radiation. The measured peak realized gain values for the wideband mode range from 2 to 3.2 dBic while the maximum gain for the narrowband mode ranged from 1.95 to 3.1 dBic. The measured results show that the proposed filtenna is suitable for UWB cognitive radio systems.**

***Index Terms*—Circularly polarized antenna, cognitive radio, microstrip slot antenna, reconfigurable antenna**

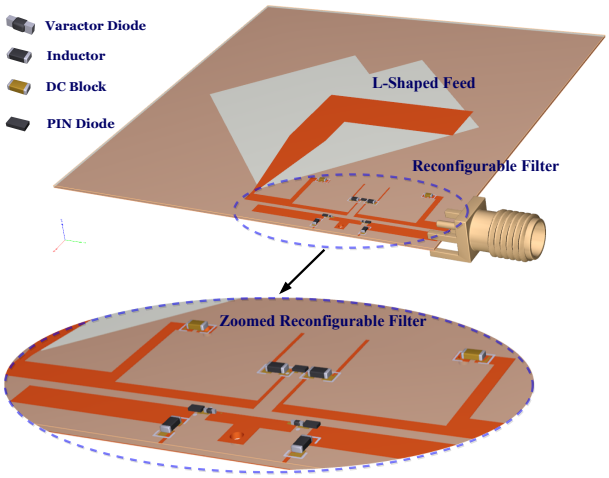

Fig. 1: Proposed reconfigurable CP antenna.

I. INTRODUCTION

DUE to the recent advancements in wireless communications, antennas have been utilized in various applications such as RFID [1], industrial communication [2], biomedical devices [3] and cognitive radio systems [4]. Due to the increasing demand for high-speed data rates requiring high resources, such as frequency bandwidth and energy, cognitive radio (CR) is a promising solution. The dynamic spectrum access ability of cognitive radio improves frequency spectrum utilization in industrial communication systems [5]. For instance, in [6] a cognitive radio sensor network has been designed to achieve reliable and efficient remote control and monitoring in smart grids. CRs employ wideband antennas to sense the occupancy of the entire spectrum (the spectrum sensing state) and are autonomously tailored to the primary transmission through narrowband antennas (the communication state). Several antennas with frequency agility [7-11], reconfigurable pattern [12,13] for CR applications have been proposed. However, there are two drawbacks that limit their capabilities. First, the use of linearly polarized antennas can lead to cross-polarization issues between transmitting (TX) and receiving (RX) antennas which can be extremely challenging for CR applications. Second, regarding dynamic spectrum access, the reported tuning range of the communicating state in previous works does not exceed 50% of the sensing state. To address the cross-polarization issue, a few works [14-16] investigated reconfigurable circularly polarized (CP) antennas as a suitable candidate for the CR, as they are less likely to be affected by multipath interferences and Tx/Rx misalignment. In [14] and [15], the proposed antennas only partially cover the sensing spectrum in the communicating state. The antenna proposed in [16] resolves this spectrum coverage issue; however it only operates at fixed pre-defined narrowband modes with no tuning ability. In this paper, to tackle both of the above limitations, we propose a reconfigurable CP slot antenna with a continuous tuning range over a wide frequency spectrum. As illustrated in Fig. 1, the perturbed square slot antenna is integrated with a switchable feed network. The feed network with three switchable modes of wideband, tunable narrow bandpass (BP) and tunable bandstop (BS) can provide the secondary user with the ability to adapt to the dynamic nature of spectrum holes while canceling any interference within the already occupied frequency band. The novel aspects of this design can be identified as a combination of all the following features in a single reconfigurable system: (a) the proposed wideband CP slot antenna can alleviate multipath interferences and misalignment between transmitter and receiver, (b) the wide continuous tuning range of the proposed CP antenna

S. Bahrami and H. -J. Song are with the Department of Electronical Engineering, Pohang University of Science and Technology, 37673 Pohang, Korea (e-mail: bahramis@postech.ac.kr; hojin.song@postech.ac.kr)

Gh. Moloudian and J. L. Buckley are with the Tyndall National Institute, University College Cork, Cork City, Ireland (e-mail: gh.moloudian@tyndall.ie, john.buckley@tyndall.ie)

This article has been accepted for publication in a future issue of this journal, but has not been fully edited. Content may change prior to final publication. Citation information: DOI 10.1109/TAP.2022.3161358, IEEE Transactions on Antennas and Propagation

covers 80% of the sensing spectrum which is significantly larger than previously reported works, (c) the tunable BS mode capability enables a wideband spectrum allocation to a secondary transceiver and avoids the interference caused by congested wireless communications applications.

This paper is organized as follows. In section II the circularly polarized antenna design is investigated. The synthesis procedure of the reconfigurable filter is then discussed in detail in section III. Simulation and measurement results of the proposed microstrip filtenna are presented in section IV. Finally, conclusions are drawn in Section V.

II. CIRCULARLY POLARIZED SLOT ANTENNA

The square slot antenna is a promising candidate to achieve ultrawideband impedance and CP bandwidth. Fig. 2(a) depicts the geometry of the reference microstrip slot antenna [17]. It is printed on two sides of a 32-mil-thick RO4003C substrate (dielectric constant $\varepsilon_r = 3.38$, $\tan\delta = 0.0009$). The top layer is a 60 mm $\times$ 60 mm microstrip square composed of a rotated square slot with a side length of a=32 mm. The bottom layer is a bent L-shaped feed connected to a 50Ω–microstrip line (Fig. 2(a)). The dimensions of the feed line are tuned to achieve a wide overlap bandwidth and excite the slot with a suitable phase to generate CP. In order to optimize the impedance matching bandwidth and CP radiation characteristics, the square slot is perturbed at the top corner. The rectangular perturbation has a width of b = 8.5 mm and a length of c = 7.5 mm. The HFSS software is used to simulate and design the proposed antenna. The S_{11} and axial ratio (AR) results for the square slot and the perturbed slot antenna are shown in Fig. 2(b). The perturbed slot antenna has a wider impedance and AR bandwidth in comparison to the square slot antenna. The proposed antenna attains a -10 dB impedance bandwidth and an AR bandwidth of 92.3 % (3.5-9.5 GHz) and 88.3 % (3.1-8 GHz), respectively. Its overlapped bandwidth, which is the bandwidth satisfying both AR <3 dB and the reflection coefficient < -10 dB is 78.2 % (3.5-8 GHz). To explain the circular polarization behavior of the proposed antenna, Fig. 3 shows the surface current vectorial distribution at 6 GHz. In this figure, the red arrows represent the direction of the locally predominant surface current and the blue arrows show the resultant of surface currents which rotates 90 degrees counterclockwise in each time step. Thus, right-hand CP (RHCP) radiation is expected for the proposed UWB slot antenna.

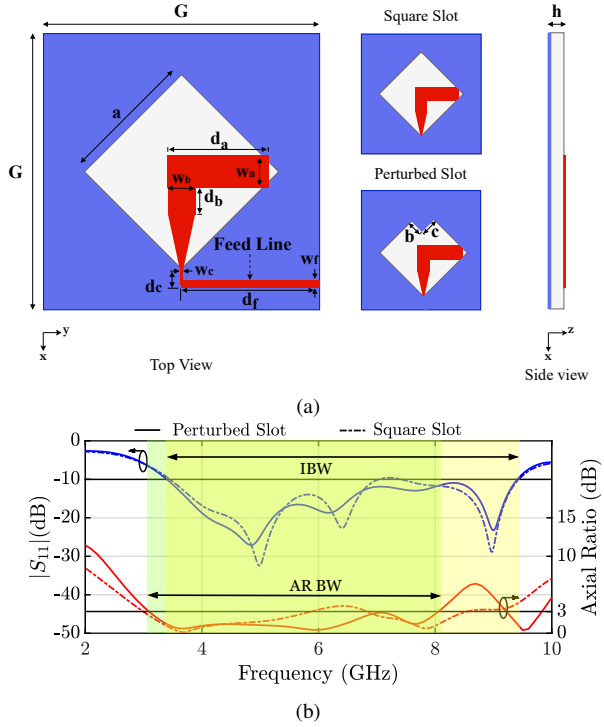

Fig. 2: Microstrip slot antennas (a) geometry (Units: mm, G=60, a=32, b=8.5, c=7.5, d_a=23.2, d_b=5.5, d_c=4.3, d_f=1.6, w_a=7, w_b=6, w_c=0.5, w_f=30.25), (h=32 mil, ε_r=3.38), (b) reflection coefficient and axial ratio.

III. RECONFIGURABLE FILTER DESIGN

Since an antenna satisfying the requirements of CP radiation and ultrawideband performance has been obtained, the next step is to design a reconfigurable filter with wide continuous tuning range within the specified bandwidth of the antenna. The substrate used for the proposed filter is the same as the substrate used for the perturbed slot antenna.

A. Ultrawideband Bandpass Filter

The proposed ultra-wide bandpass filter (BPF) consists of two shunt short-ended stubs and three cascaded line sections in the middle. All the series and shunt sections are set with the same electrical length as $\pi/2$ at center frequency f_0. The Chebyshev response with equal-ripple in-band behavior and a pair of transmission zeros at $\pm\alpha$ can be calculated by the proposed method in [18].

$$|\mathbf{S}_{21}|^2 = \frac{1}{1+\varepsilon^2\cos^2(3\phi+\xi)} \tag{1}$$

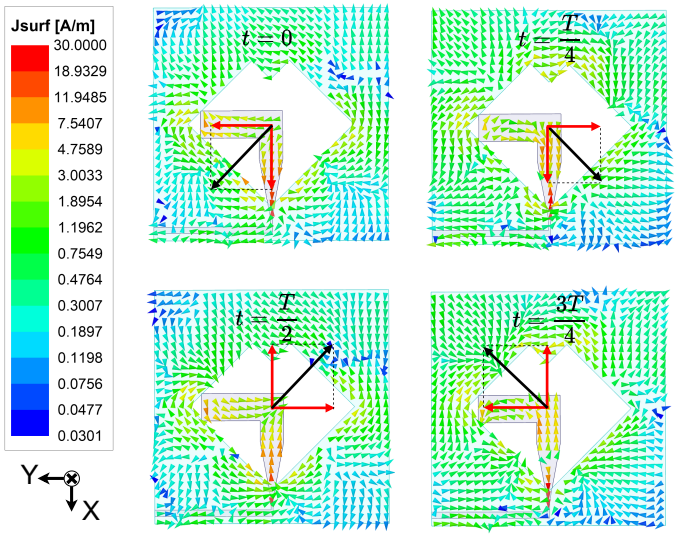

Fig. 3: Simulated surface current distributions of the slot antenna at 6 GHz.

This article has been accepted for publication in a future issue of this journal, but has not been fully edited. Content may change prior to final publication. Citation information: DOI 10.1109/TAP.2022.3161358, IEEE Transactions on Antennas and Propagation

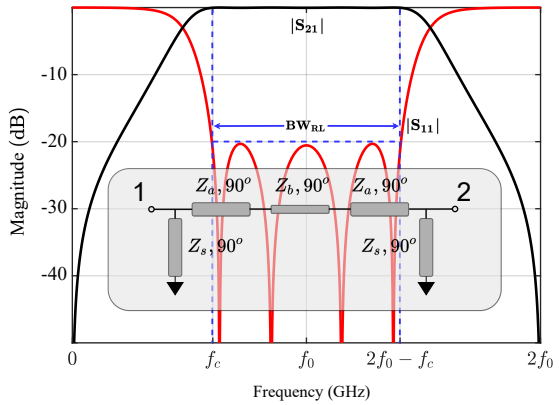

Fig. 4: The frequency response of the microstrip ultrawideband filter, (inset) layout.

and

$$x = \alpha \cos\theta \quad (2)$$

$$\phi = \cos^{-1}(x) \quad (3)$$

$$\xi = \cosh^{-1}[x\sqrt{(\alpha^2-1)(\alpha^2-x^2)}] \quad (4)$$

Where $\alpha = 1/\cos\theta_c$ (θ_c is the electrical length at lower cutoff frequency f_c) and ε is the equal-ripple constant in relevance to the specified return loss RL (dB) [19-20]. The upper cutoff frequency of this bandpass filter appears at $(\pi - \theta_c)$. Thus, the return-loss bandwidth $\mathrm{BW_{RL}}$ in Fig. 4 can be expressed as

$$\mathrm{BW_{RL}} = \frac{2(f_0 - f_c)}{f_0} = \frac{(\pi - 2\theta_c)}{\pi/2} \quad (5)$$

As a result, the characteristic impedances of individual sections can be explicitly determined once the return loss and the fractional bandwidth are specified.

B. T-shaped Resonator

Varactor-based structures are widely used in tunable filter designs [21]. The frequency-agile bandpass filter design is inspired by a synchronously tuned dual-mode resonator proposed in [22]. A much wider tuning range of operation can be added to this design based on optimization of resonators impedances in each section (2 arms of the T-shaped resonator and central part, separately). The modified T-shaped resonator with a shorted stub is loaded by two varactors to control the center frequency of the BPF (Fig. 5). This architecture was primarily used as a BPF. However, as presented in [12], a tunable BS mode of operation can be introduced to this design.

C. Triple-mode Reconfigurable Filter

The modified T-shaped narrowband resonator and the introduced UWB filter are integrated to form a composite reconfigurable filter, as illustrated in Fig. 5. For the wideband state (3.5-8.5 GHz), the characteristic impedances for the shunt short-ended stubs (Z_s) and cascaded line sections of the UWB BPF (Z_a, Z_b) are determined. Without affecting the overall performance of the UWB BPF, short-ended shunt stubs and the middle high impedance line (Z_b) are meandered. A PIN

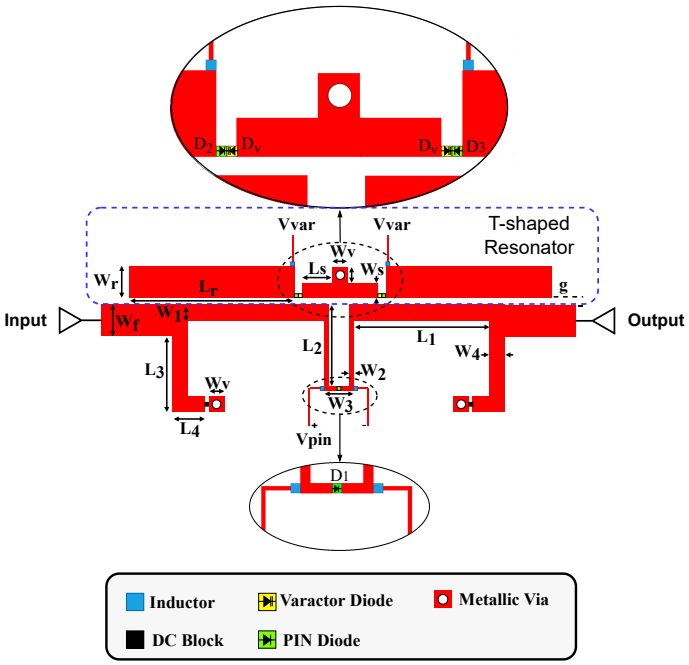

Fig. 5: Geometry of the proposed reconfigurable filter (Units: mm, W_1=0.75, W_2=0.2, W_3=1.4, W_4=0.78, W_r=1.7, W_f=1.6, W_v=0.78, W_s=0.85, L_1=8.5, L_2=3.8, L_3=5.8, L_4=1.85, L_r=10.4, L_s=1.65, g=0.65).

diode ($\mathbf{D_1}$) is inserted in the middle of the high impedance line to control the direct input/output path.

The modified T-shaped narrowband resonator is located halfway between the input and output ports on the top side. Two PIN diodes $\mathbf{D_2}$, and $\mathbf{D_3}$ are placed into both halves of the coupled-line sections of this T-shaped resonator. The PIN diodes are MACOM MA4GP907 which have an on-resistance of 4 Ohms (at 1 GHz) and an off-capacitance of 0.025 pF (at 1 MHz) [9]. The DC bias lines (V_{pin}) for these diodes are connected to one end of an RF blocking 56 nH coil inductor. The forward bias current of the PIN diodes is 10 mA. Meanwhile, the MACOM MA46580 varactor diode was selected for controlling the tuning range of the modified T-shaped narrowband resonator. It can be considered as the series RLC equivalent circuit according to its datasheet (Fig. 6 (a)). The equivalent circuit is composed of a series resistance (R=1.75 Ω), a parasitic inductance (L=0.4 nH), and a total capacitance (C=0.08 pF). The tuning reverse bias voltage of the diode (V_{var}) can be varied from 2 to 12 V, with a resulting change in capacitance C in the range from 0.15 to 2.1 pF. When diode $\mathbf{D_1}$ is turned OFF, while $\mathbf{D_2}$, and $\mathbf{D_3}$ are turned ON, the proposed filter operates in its narrowband BP state. In this case, the power is transmitted through the modified T-shaped narrowband resonator. In contrast, when all the PIN diodes are turned ON, the reconfigurable filter operates in its narrowband BS state. If the PIN diodes $\mathbf{D_2}$ and $\mathbf{D_3}$ are turned OFF, while $\mathbf{D_1}$ is turned ON, the reconfigurable filter operates in its wideband state. By varying the bias voltage of the two varactor diodes, one can continuously shift the bandpass/stop frequencies from 4.3 to 8.2 GHz. By optimizing the impedance

This article has been accepted for publication in a future issue of this journal, but has not been fully edited. Content may change prior to final publication. Citation information: DOI 10.1109/TAP.2022.3161358, IEEE Transactions on Antennas and Propagation

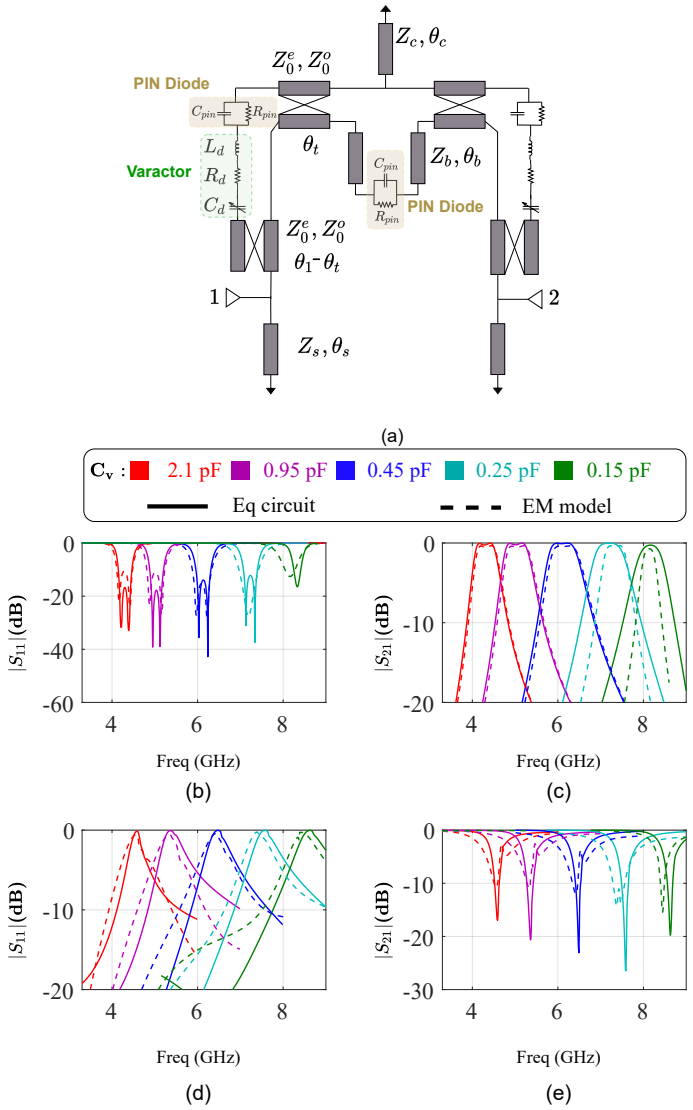

Fig. 6: Comparison of the S-parameter simulation results for the equivalent circuit and the EM models. (a) Equivalent circuit of the proposed reconfigurable filter, (b, c) the BPF narrowband mode, (d, e) the BSF narrowband mode.

of T-shaped resonator arms and incorporating this type of varactor diode a much wider tuning range is obtained. The proposed filter modes of operation are listed in Table I. The performance of the reconfigurable filter has been simulated using HFSS. Fig. 6(b, c) and (d, e) give the S parameter results for the BP narrowband mode and the BS narrowband mode, respectively. When the capacitance of the varactors varies from 0.15 to 2.1 pF, the passband of the filter operating in BP mode is tuned from 4.3 to 8.2 GHz. On the other hand, the stopband of the filter operating in BS mode is tuned from 4.5 to 8.5 GHz.

IV. RESULTS AND DISCUSSION

A photograph of the fabricated prototype frequency tunable antenna is shown in the inset of Fig. 7. This antenna has 3 modes of operation. The measured and simulated AR and realized gain are shown in Fig. 7(a). The out-of-band filtering

TABLE I: The operation modes of the reconfigurable filter

D_1	D_2	D_3	Operation State	Tuning Range Bandwidth
ON	ON	ON	Band Stop (Narrowband)	4.5 GHz ⇌ 8.5 GHz 200 MHz
OFF	ON	ON	Band Pass (Narrowband)	4.3 GHz ⇌ 8.2 GHz 600 MHz
ON	OFF	OFF	Band Pass (UWB)	— 5 GHz (3.5 GHz - 8.5 GHz)

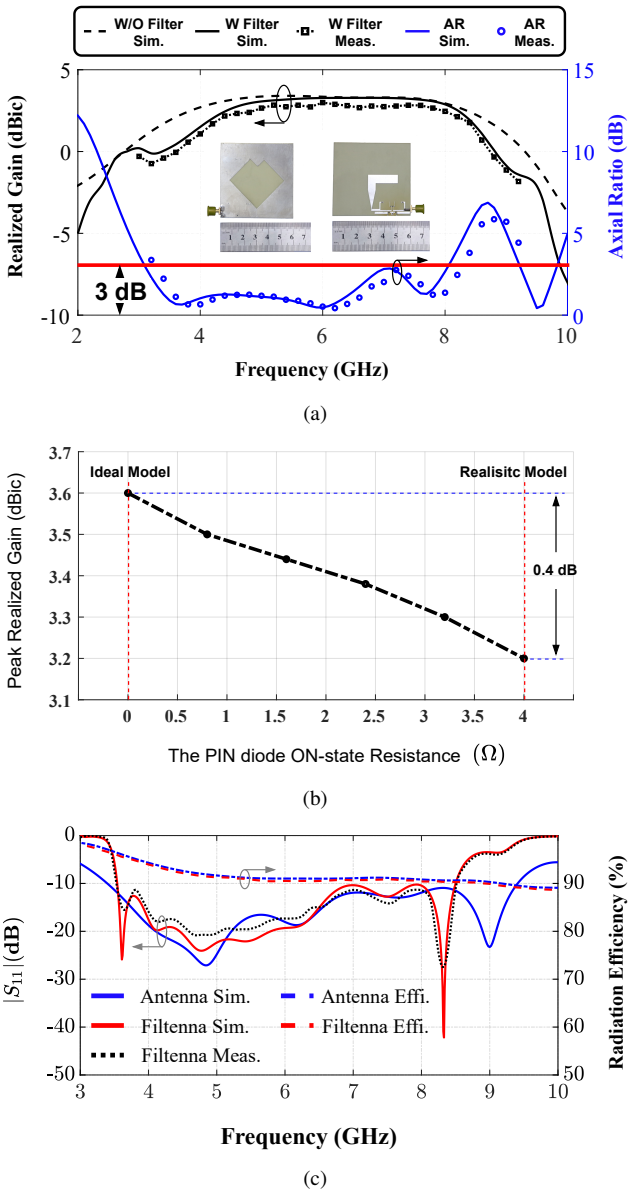

Fig. 7: Measured and simulated results when the filtenna is in its wideband mode (a) Peak realized gain and AR, (inset) the fabricated filtenna, (b) the peak realized gain versus the PIN diode ON-state resistance, (c) $|S_{11}|$ and the radiation efficiency

This article has been accepted for publication in a future issue of this journal, but has not been fully edited. Content may change prior to final publication. Citation information: DOI 10.1109/TAP.2022.3161358, IEEE Transactions on Antennas and Propagation

TABLE II: Comparison of the proposed antenna with some published antennas featuring reconfigurable response.

Refs.	Dielectric Constant	WideBand Mode (Sensing band)		Discrete/ Continuous	Tuning Range (CM band) (GHz)	Ratio of Tuning range to Sensing BW	Modes of Operation	Polarization	Size (λ_0^2)
		IBW (GHz)	AR-BW (GHz)						
[9]	3.48	2.35-4.98	N/A	C	3.05-4.39	50.95 %	WB-BP	Linear	0.23×0.39
[11]	2.2	3.10-10.6	N/A	C	3.1-5.6	33.33 %	WB-BP	Linear	0.75×0.65
[12]	3.38	3-7.5	N/A	C	3.31-5.53	50.4 %	BP-BS	Linear	0.75×0.7
[13]	3.38	2.51-6.24	N/A	C	3.3-5.58	51.3 %	WB-BP-BS	Linear	1.24×1.65
[14]	4.6	2-8	2-3.2	D	5.8	N/A	WB-BP	Circular	1×1.15
[15]	4.4	1.6-2.56	1.62-2.55	D	1.275/2.35	N/A	WB-BP	Circular	0.35×0.35
[16]	3.38	3-11.57	3.1-8	D	3.59/5.45	N/A	WB-BP	Circular	0.61×0.68
This work	**3.38**	**3.5-8.5**	**3.5-8**	**C**	**4.5-8.5**	**80 %**	**WB-BP-BS**	**Circular**	$\mathbf{0.7 \times 0.7}$

IBW: -10 dB Impedance Bandwidth CM: Communications BS: Narrowband Bandstop Mode
AR-BW: 3 dB Axial Ratio Bandwidth WB: Wideband Mode BP: Narrowband Bandpass Mode N/A: Not Applicable

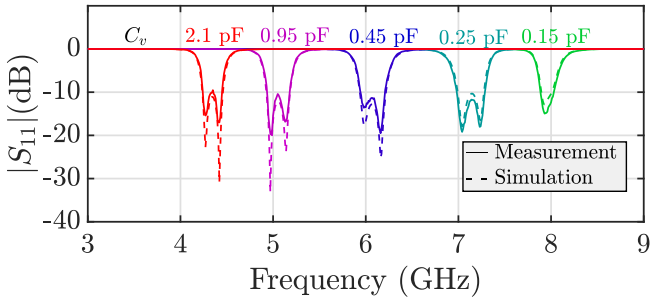

Fig. 8: Measured and simulated $|S_{11}|$ vs frequency when the filtenna is in its narrowband BP mode.

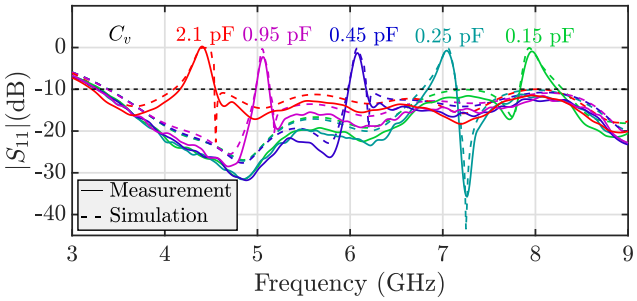

Fig. 9: Measured and simulated $|S_{11}|$ vs frequency when the filtenna is in its BS mode.

can be seen in comparison to the stand-alone antenna. It is notable that the resistance of the PIN diode in the ON state slightly degrades the efficiency and the gain of the antenna [23]. Based on the simulation results shown in Fig. 7(b), the peak realized gain reduced by 0.4 dB when the ideal PIN diode is replaced by the realistic model. Also, the measured AR bandwidth is 85 % (3.3-8.2 GHz). The total antenna size is 60 mm $\times$ 60 mm corresponding to $0.7\lambda_0 \times 0.7\lambda_0$ (λ_0 is the wavelength at the lowest operating frequency). The scattering parameters at the input port of the filtenna in its wideband mode of operation are depicted in Fig. 7(c). The measured and simulated reflection coefficient of the antenna in its narrow bandpass mode are illustrated in Fig. 8. The varactor capacitances (bias voltages) are vary from 0.15 pF (12 V) to 2.1 pF (2 V) with the reflection coefficient less than -10 dB for the tuning range of 4.3 GHz to 8.2 GHz (4.35 to 8.3 GHz). To activate the narrow bandstop mode all PIN diodes are switched ON and accordingly the notch frequency is tuned, by altering the varactor capacitances, from 4.5 to 8.5 GHz, as illustrated in Fig. 9.

The simulated and measured realized gains and AR of the proposed antenna for the narrowband modes are shown in Fig. 10. The realized gain values were measured by changing the varactors bias voltage. The measured maximum gain for the narrowband BP mode ranged from 2 to 3.1 dBic. The AR values remaind under 3 dB in the specified tuning range. Table II compares the performance of the proposed antenna with other tunable antennas. The main advantage of the proposed antenna system is its wide continuous tuning range (4.5-8.5 GHz), covering 80% of the sensing spectrum which is significantly higher than previously reported works. Moreover, the BS mode of operation provides an additional wideband

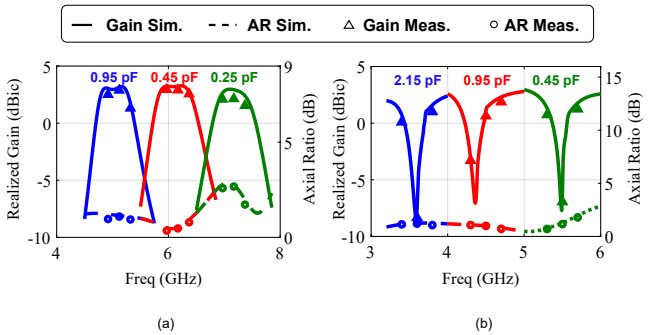

Fig. 10: Simulated and measured realized gains and AR of the filtenna versus frequency, (a) bandpass filter mode, (b) bandstop filter mode.

communicating state while avoiding the potential interference caused in crowded wireless communications applications. Fig. 11 shows the measured and simulated normalized radiation patterns at 4.5, 6.0, and 7.5 GHz (XZ-Plane and YZ-Plane) for the wideband of operation. The asymmetrical design of the proposed antenna structure gives rise to tilted radiation patterns. The radiation pattern falls to zero in approximately perpendicular direction to the maximum due to the cancellation effect of surface currents at higher-order modes. The radiation patterns of the proposed CP antenna on both sides are almost the same. In other words, as CP slot antennas radiate bidirectional wave, the front-side radiates RHCP while the back-side radiates LHCP.

V. CONCLUSION

In this paper, we proposed a CP reconfigurable filtenna with a switchable integrated feed network. The choice of the CP antenna for cognitive radio application is very effective in

This article has been accepted for publication in a future issue of this journal, but has not been fully edited. Content may change prior to final publication. Citation information: DOI 10.1109/TAP.2022.3161358, IEEE Transactions on Antennas and Propagation

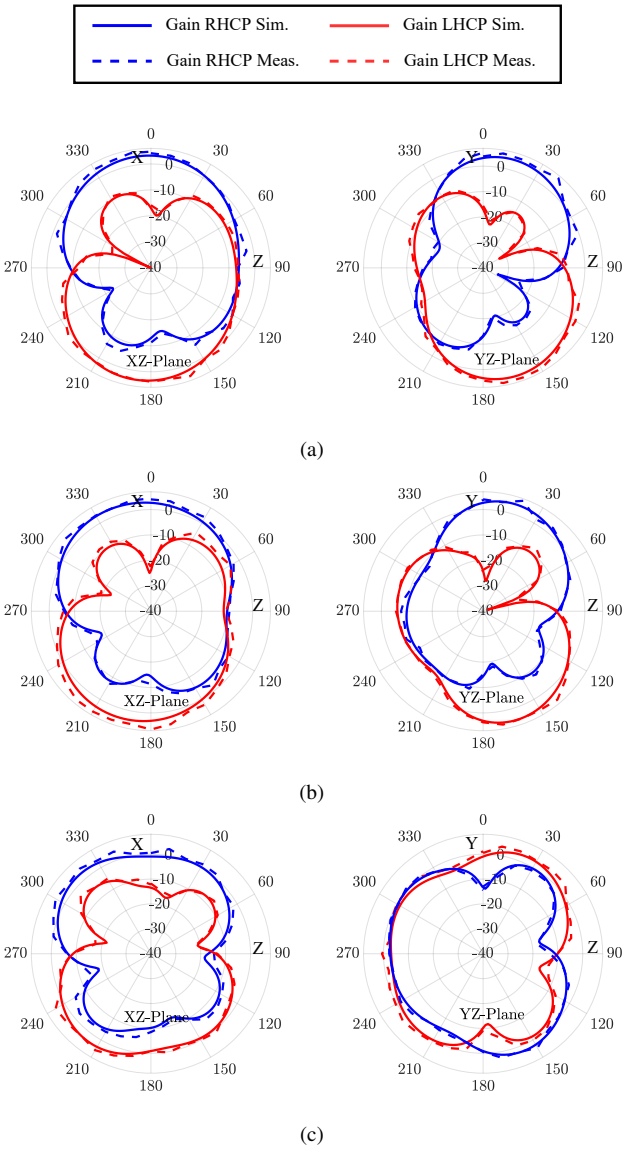

Fig. 11: Simulated and measured radiation patterns for the proposed filtenna in its wideband mode (a) 4.5 GHz, (b) 6 GHz, (c) 7.5 GHz.

overcoming multi-path interference. Also, the wide continuous tuning range (4.5-8.5 GHz) of the proposed antenna is advantageous. The integrated feed network is composed of a 50 Ω microstrip line, an ultra-wideband (UWB) BPF and a T-shaped resonator. The RF signals propagate through different paths that are configured using three PIN diodes, to achieve frequency reconfiguration. The continuous tuning range of the BS/BP narrowband modes is controlled by two DC-controlled varactor diodes. The additional narrow BS mode of operation gives the proposed structure a more versatile communicating state. The measured results show that the proposed antenna is suitable for a wide range of cognitive radio applications.

REFERENCES

[1] Y. Yao, Y. Liang, J. Yu and X. Chen, "Design of a Multipolarized RFID Reader Antenna for UHF Near-Field Applications," *IEEE Trans. Antennas Propag.*, vol. 65, no. 7, pp. 3344–3351, July 2017.

[2] O. Jo, W. Kwon and W. Hong, "Achieving 360 Degree Coverage Dynamic and Switchable Beamforming through Resource-Efficient Switchable Antennas for Future mmWave IoT Devices," *IEEE Trans. Ind. Electron.*, doi: 10.1109/TIE.2020.3020022.

[3] S. Bahrami, G. Moloudian, S. R. Miri-rostami and T. Bjorninen, "Compact Microstrip Antennas with Enhanced Bandwidth for the Implanted and External Subsystems of a Wireless Retinal Prosthesis," *IEEE Trans. Antennas Propag.*, vol. 69, no. 5, pp. 2969–2974, May 2021.

[4] Y. Tawk, J. Costantine and C. G. Christodoulou, "Cognitive-radio and antenna functionalities: A tutorial [Wireless Corner]," *IEEE Antennas Propag Mag*, vol. 56, no. 1, pp. 231–243, Feb. 2014.

[5] H. M. E. Misilmani, M. Y. Abou-Shahine, Y. Nasser, and K. Y. Kabalan, "Recent Advances on Radio-Frequency Design in Cognitive Radio," *Int. J. Antennas Propag.*, vol. 2016, pp. 1–6, Feb. 2016.

[6] C. You et al., "Study of RF Subsystem Used in Dynamic Spectrum Sharing System at TV Band," *IEEE Trans. Ind. Electron.*, vol. 60, no. 6, pp. 2346–2357, June 2013.

[7] J. Deng, S. Hou, L. Zhao and L. Guo, "Wideband-to-Narrowband Tunable Monopole Antenna With Integrated Bandpass Filters for UWB/WLAN Applications," *IEEE Antennas Wirel. Propag. Lett.*, vol. 16, pp. 2734–2737, 2017.

[8] B. Liu, J. Qiu, S. Lan and G. Li, "A Wideband-to-Narrowband Rectangular Dielectric Resonator Antenna Integrated With Tunable Bandpass Filter," *IEEE Access*, vol. 7, pp. 61251–61258, 2019.

[9] M. Tang, Z. Wen, H. Wang, M. Li and R. W. Ziolkowski, "Compact, Frequency-Reconfigurable Filtenna With Sharply Defined Wideband and Continuously Tunable Narrowband States," *IEEE Trans. Antennas Propag.*, vol. 65, no. 10, pp. 5026–5034, Oct. 2017.

[10] M. R. Hamid, P. Gardner, P. S. Hall and F. Ghanem, "Switched-Band Vivaldi Antenna," *IEEE Trans. Antennas Propag.*, vol. 59, no. 5, pp. 1472–1480, May 2011.

[11] A. K. Horestani, Z. Shaterian, J. Naqui, F. Martín and C. Fumeaux, "Reconfigurable and Tunable S-Shaped Split-Ring Resonators and Application in Band-Notched UWB Antennas," *IEEE Trans. Antennas Propag.*, vol. 64, no. 9, pp. 3766–3776, Sept. 2016.

[12] S. Malakooti, S. M. H. Mousavi and C. Fumeaux, "Tunable Bandpass-to-Bandstop Quasi-Yagi–Uda Antenna With Sum and Difference Radiation Patterns," *IEEE Trans. Antennas Propag.*, vol. 67, no. 4, pp. 2260–2271, April 2019.

[13] S. Malakooti and C. Fumeaux, "Pattern-Reconfigurable Antenna With Switchable Wideband to Frequency-Agile Bandpass/Bandstop Filtering Operation," *IEEE Access*, vol. 7, pp. 167065–167075, 2019.

[14] F. D. Dahalan et al., "Frequency-Reconfigurable Archimedean Spiral Antenna," *IEEE Antennas Wirel. Propag. Lett.*, vol. 12, pp. 1504–1507, 2013.

[15] I. H. Idris, M. R. Hamid, K. Kamardin, and M. K. A. Rahim,"A multi to wideband frequency reconfigurable antenna," *Int. J. RF Microw. Comput. Aided Eng.*, vol. 28, no. 4, 2018, Art. no. e21216.

[16] M. E. Yassin, H. A. Mohamed, E. A. F. Abdallah and H. S. El-Hennawy, "Circularly Polarized Wideband-to-Narrowband Switchable Antenna," *IEEE Access*, vol. 7, pp. 36010–36018, 2019.

[17] K. Agarwal, Nasimuddin and A. Alphones, "Unidirectional wideband circularly polarised aperture antennas backed with artificial magnetic conductor reflectors" *Microw. Antennas Propag.*, vol. 7, no. 5, pp. 338–346, Apr. 2013.

[18] Y. Lyu, L. Zhu and C. Cheng, "Single-Layer Broadband Phase Shifter Using Multimode Resonator and Shunt $\lambda/4$ Stubs," *IEEE Trans. Compon. Packag. Technol.*, vol. 7, no. 7, pp. 1119–1125, July 2017.

[19] R. Li, S. Sun and L. Zhu, "Synthesis Design of Ultra-Wideband Bandpass Filters With Composite Series and Shunt Stubs," *IEEE Trans. Microw. Theory Tech.*, vol. 57, no. 3, pp. 684–692, March 2009.

[20] M. K. Alizadeh, H. Shamsi, M. B. Tavakoli, and H. Aliakbarian, "Simple ladder-like single-layer balanced wideband phase shifter with wide phase shift range and appropriate common-mode suppression," *IET Digit. Library*, vol. 14, no. 10, pp. 1137—1147, Aug. 2020.

[21] G. Moloudian, S. Bahrami and R. M. Hashmi, "A Microstrip Lowpass Filter With Wide Tuning Range and Sharp Roll-Off Response," *IEEE Trans. Circuits Syst. II: Express Br.*, vol. 67, no. 12, pp. 2953–2957, Dec. 2020.

[22] D. Lu, N. S. Barker and X. Tang, "A Simple Frequency-Agile Bandpass Filter With Predefined Bandwidth and Stopband Using Synchronously Tuned Dual-Mode Resonator," *IEEE Microw. Wirel. Compon. Lett.*, vol. 27, no. 11, pp. 983–985, Nov. 2017.

[23] M. Shirazi, T. Li, and X. Gong, "Effects of PIN diode switches on the performance of reconfigurable slot-ring antenna," in *Proc. IEEE 16th Annu. Conf. Wireless Microw. Technol.*, Apr. 13—15, 2015, pp. 1—3.